A micro finite element model for soil behaviour: experimental evaluation for sand under triaxial compression

S. Nadimi[1], J. Fonseca[2]*, E. Andò[3], G. Viggiani[3]

*Corresponding Author

Joana.Fonseca.1@city.ac.uk

ABSTRACT

This paper evaluates the ability of a combined discrete-finite element approach to replicate the experimental response of a dry sand under triaxial compression. The numerical sample was created by virtualising the fabric of a Martian regolith-like sand sample obtained from an *in-situ* test using X-ray micro Computed Tomography and physical properties of the grains obtained from laboratory data were used as input. The boundary and contact conditions were defined according to the experimental test. A key feature of the model is the use of deformable thin-shell elements to represent the numerical membrane, which allows for a realistic failure mode and volumetric deformation. The macroscopic response of the numerical simulation is shown to compare well with the experiment. The contact regions are identified based on their ability to transmit stress and the evolution of the contact normals is shown to correlate well with the macro stress evolution. The computed stress fields within each grain are used to identify the load bearing grains in the assembly, contributing new insights beyond the commonly reported force chains.

KEYWORDS

Fabric/structure of soils; Particle-scale behaviour; Numerical modelling; Sands; Triaxial test

[1] School of Engineering, Newcastle University, UK (formerly City, University of London)

[2] Department of Civil Engineering, City, University of London, UK

[3] Université Grenoble Alpes, CNRS, Grenoble INP, 3SR, F-38000 Grenoble, France

INTRODUCTION

Improving computational modelling towards a more realistic description of granular behaviour is a long standing challenge (*e.g.* O'Sullivan, 2011; Matsushima & Chang, 2011; Andrade, *et al*., 2012; Kawamoto, *et al*., 2018). Nadimi & Fonseca (2018a, 2018b) proposed a micro Finite Element (μFE) model that virtualises the fabric of a natural sand obtained from micro Computed Tomography (μCT) to simulate the mechanical response under loading. In this model, the grain-to-grain interactions are modelled in a framework of combined discrete-finite element method (Munjiza, 2004). The underlying idea for the development of this μFE model was the need to better represent soil fabric into numerical modelling. The effect of fabric on the mechanical response of soil is well-known and has been repeatedly demonstrated in both experiments and numerical analysis (e.g., Cuccovillo & Coop, 1999; Oda & Iwashita, 1999; Kuwano & Jardine, 2002; Ng, 2004; Fonseca, *et al*., 2016).

A complete three-dimensional (3D) description of the grains morphologies and their geometrical arrangement can be effectively obtained from μCT scanning (e.g., Hall, et al., 2010; Fonseca, *et al*., 2013; Vlahinić, *et al*., 2013). Further, by making use of advanced image processing and meshing techniques, the individual grains can be identified in the 3D images and meshed to create numerical (deformable) grains that replicate the real ones. This aspect is significant for modelling grain-to-grain contact interaction in an assembly. In fact, contact response has a strong dependency on the grain shape as demonstrated in Nadimi & Fonseca (2017) for a series of tests on both silica and carbonate grains. Michalowski, *et al*. (2017) also showed through single grain experiments that contact response for natural grains does not follow a Hertzian response due to the effect of shape. In the μFE framework used here, the contact response originates from the deformation of the grain, which constitutes an important advance when compared with the rigid body assumption and the associated pre-defined contact laws used in most discrete element approaches. Another advantage of using deformable grain is the ability to compute the stress and strain fields within the grain which is critical to the understanding of yield initiation and crack propagation. Although this enhancement to simulate breakage is yet to be included in the model, this does not constitute an issue for the simulation of an assembly of grains under relatively low load as the case reported here.

Here, the μFE model is evaluated against the results of a triaxial compression experiment. One of the challenges in numerical modelling of triaxial tests is the correct representation of the boundary conditions, i.e. the sample membrane for the case of a triaxial test (Cui *et al*., 2007; Cheung & O'Sullivan, 2008). In triaxial compression simulations, the numerical membrane should enable the specified confining pressure to be applied to the sample, while non-restricting grain rearrangement. De Bono, *et al*. (2012) proposed a cylindrical wall formed by bonded spheres to represent the membrane. Using bonded spheres, however, has the drawback of restraining rolling and translation of the grains near the membrane, as well as enabling grain

penetrate though the membrane (depending on the relation between the size of the grains and the size of the bounded spheres). Despite the limitations of using flexible membranes to simulate triaxial tests in DEM they are still widely used as demonstrated by a number of the recent studies (e.g., Lu et al., 2018; Khoubani & Evans, 2018; Zhang et al, 2018; Binesh et al., 2018). An alternative approach using shell elements (Ahmad et al., 1970; Reese et al. 2001; Sze, 2002) to represent the membrane is discussed in this study.

The term 'force chains' is widely used in granular mechanics to describe filamentary patterns of grains transmitting above average contact forces (*e.g.* Majmudar & Behringer, 2005; Radjai, *et al*., 2017). Only a handful of studies have used the 'stress chain' concept (Gerritsen, *et al*., 2008; Maeda *et al*., 2010; Blumenfeld & Ma, 2017). When dealing with irregular shaped grains that are prone to form contact through an area (in some cases, large) rather than a point as for perfect spheres, the discussion on whether to use force or stress to identify the heavily loaded grains becomes pertinent. The aims of this paper are twofold. To carry out a numerical simulation able to replicate the bulk experimental response of a sand under triaxial compression using as input parameters only experimental measured data. Further, to contribute with alternative micro-scale measures more suitable for irregular shaped grains, such as the already mentioned stress-chains but also the concept of active contact based on the transmission of load rather than geometric-based analysis. The present study investigates, for the first time, the formation of columns of load bearing grains using both force and stress quantities. In addition, the evolution of contact forces through deformation is linked to grain kinematics to investigate the role of force network in the stability of the granular assembly.

THE µFE MODEL

The µFE model used here combines four techniques: (i) image acquisition and processing; (ii) image-based mesh generation; (iii) finite element solver, and (iv) discrete element solver. The 3D images are acquired using X-ray µCT and the individual grains are segmented using a watershed approach as described in Kong & Fonseca (2018). The numerical approximation of the problem starts from discretising an object into a collection of elements and nodes. A Delaunay refined algorithm is employed to extract the grain iso-surface (Shewchuk, 2014). The grain is then filled with tetrahedral elements for the sub-volumes bounded by the iso-surfaces to obtain the 3D mesh. The generated mesh is imported into the combined finite-discrete numerical domain. More details can be found in Nadimi & Fonseca (2018 a, b).

In the numerical domain, the nodal force includes the contribution from contact forces, internal strain and external loads. A grain can locally deform depending on the current nodal forces enabling a stress/strain field to be computed within each individual grain. The body motion for the grain is calculated using an explicit central difference integration rule. Currently, the model

runs in Abaqus finite-element package (Dassault Systèmes, 2014) and is implemented with an explicit algorithm that uses a dynamic framework.

A CASE STUDY

A case study is presented here to investigate the ability of the μFE approach to reproduce the experimental behaviour of a sample of sand under triaxial compression. The material tested is a Martian regolith-like sand also termed Eglin sand (Nardelli et al, 2017). From the microscale characterisation carried out by Nardelli and co-authors, the median grain size is 1.2 mm and the constituent grains display various colours from black, to pink-yellow, to grey-transparent according to their chemical/ mineralogical composition. The average sphericity values vary between 0.5-0.8 and the roundness are within the rage of 0.4-0.5, according to visual observations using Krumbein and Sloss chart (Krumbein and Sloss, 1963).

Experiments

The sand specimen with 11 mm diameter and 22 mm height was first compressed isotropically to 100 kPa and subsequently subjected to displacement controlled axial loading with a strain rate of 0.1%/min under constant confining pressure. The test was performed inside a μCT scanner to image the internal structure of the specimen (*e.g.* Andò, *et al*., 2012). The sample was prepared by air pluviation and an initial void ratio of 0.56 was measured. The 3D images were acquired at a voxel size of 15.5 μm, which means that a grain with a median diameter of 1.2 mm is represented by approximately 70 voxels across its diameter. Following image segmentation, 3,158 individual grains were identified in the specimen.

Numerical modelling

The 3D image of the specimen prior to loading was meshed and each voxel in the images was converted into Cartesian coordinates. The specimen is represented in the numerical domain by a total of 10,105,720 elements comprising 3,503,151 nodes. The elastic material model was assigned to the grain with Young's modulus E=70 GPa and Poisson ratio ν=0.3. The coefficient of friction used was of 0.28, obtained from single grain experiments on this material, more details of the tests can be found in Nardelli et al. (2017). Nardelli and co-authors carried out a detailed characterization of the grains according to their mineralogical classes. In addition they reported an overall mean inter-particle friction angle for all the particles of 17.7±6.9. And this was the values used here to derive the coefficient of friction since the simulation uses global values rather that grain specific parameters (something to be developed in future work). The density of the grains is also an input of the model and a value of ρ=2,500 kg/m³ was used here.

To better replicate the experimental conditions and avoid the limitations of previously used methods to represent the numerical membrane, deformable triangular thin-shell elements were used here. The properties of these elements were E=125 MPa and ν=0.49. Their sizes were set to be lower than those defining the grains and this is an important aspect for a more accurate modelling at the grain-membrane interface. A standard value of 0.2 mm was used for the thickness of the membrane. For the top and bottom platens, rigid elements were used. The numerical sample was first subjected to a confining pressure of 100 kPa and subsequently axially compressed to 10% strain under the same conditions as the experimental sample.

Comparison of the results

A view of the full numerical sample at the start and at the end of the test (10% axial strain) is shown in Figs. 1a and 1b, respectively. At the end of the test the specimen shows a slight barrelled shape and this is in agreement with the experiments, as depicted in Fig. 1c and 1d (at the stages of 0% and 10% axial strain, respectively). Two local views of the numerical sample are presented in Fig. 2 to illustrate the ability of the numerical membrane to deform around the grains under the confining pressure, mimicking the laboratory membrane.

The stress-strain response obtained from the μFE model is compared with the experimental response in Fig. 3a and the volumetric response is depicted in Fig. 3b. Overall, a good agreement can be seen. Both the experimental and numerical responses show a strain hardening phase with the numerical sample being slightly stiffer. This phase is then followed by a plateau in both experimental and numerical specimens. Regarding the volumetric response, a good agreement is also observed. In both cases there is an initial phase during which no significant change in volume occurs, followed by a clear increase in volumetric strain (dilation).

Evolution of the active contacts

The grain-to-grain contacts were identified based on the principle of 'active contacts'. This consists of defining the contact regions by using the surface nodes that have contact force higher than zero, i.e., at least one of the three components of the force (Fx, Fy, Fz) greater than zero. Relying on force measurements to identify contacts has the advantage of avoiding uncertainties, e.g. systematic contact overdetection, related to image segmentation and voxel size issues commonly found in purely geometric contact identification (*e.g.* Fonseca *et al.*, 2013; Wiebicke, *et al*., 2017).

Another advantage of this technique is that the vector defining the normal to the contact region at each node is easily obtained, which is interesting for fabric analysis (e.g. Wang et al, 2004; O'Sullivan, 2011; Fonseca et al., 2013; Yang & Wu, 2016).

Four strain levels (axial strain values of 2.5%, 5.5%, 7.5%, and 9.5%) were chosen here to investigate the evolution of the predominant orientation of the contact normal vectors and their associated contact region. The active contact area at each loading stage is directly proportional to the number of active contact vectors (one vector per element).

The distribution of the contact normal vectors is presented in Fig. 4 by means of polar plots, in this projection; the centre of the circle corresponds to an orientation parallel with the axis of the sample (i.e., the z direction). For axial strain of 2.5% (Fig. 4a) it can be seen that nearly all vectors (approximately 99%) are clustered around the middle of the plot, represented here by light shades, which corresponds to polar angle θ values between 0-10° (angle between the vector and vertical direction). The vectors distribution becomes more scattered as the polar angle θ increases and only a residual number of vectors (approximately 0.2%) exhibit a nearly horizontal orientation, i.e. a θ value greater than 65° (represented here by darker shades). For the stage of 5.5% strain (Fig. 4b) it can again be seen the clustering of the vectors in the middle region of the polar plot, the only difference is that the number of vectors is higher (22% increase in comparison with the previous stage), which explains the slight increase in the number of vectors for θ between 10°-20° (represented here by lighter shades) but this number of vectors is still insignificant when compared with the number located in the θ range of 0-10°. For the subsequent stages (Figs. 4c and 4d) the trend observed is again similar and the subtle changes in colour are mainly a result of the decrease in the number of vectors when compared with the previous stages (incremental reductions of 28% and 25%, respectively).

The alignment of the contact normal vectors in the direction of the major principal stress as deformation progresses is in agreement with the findings reported by Fonseca *et al*. (2013, 2016), for which pure geometrical considerations were used to identify the contacts and the associate normal vectors. When comparing the results from the geometrical approach and the active contacts approach, the aspect worth mentioning is the very small number of vector with orientations closer to horizontal found in the latter. Despite the sands being different (Fonseca and co-authors used an intact locked sand), this observation seems to suggest that the contacts for which the normal vector is nearly horizontal are not transmitting stress.

The degree of clustering around the direction of the major principal stress is quantified here using the anisotropy of the distribution of the contact normal, given by the difference between the maximum and minimum eigenvalues of the fabric tensor (Fonseca *et al*., 2013). The fabric tensor of the contact normal is a useful tool to describe the preferred orientation of the dataset and its associated intensity. A second-order symmetric tensor as proposed by Satake (1982) is used here:

$$\Phi_{ij} = \frac{1}{N}\sum_{k=1}^{N} n_i^k n_j^k \qquad (1)$$

where N is the total number of vectors in the system and n_i^k is the unit orientation vector along direction i. The anisotropy value obtained from Φ_1- Φ_3 will take the value *0* for an isotropic system and *1* for a highly anisotropic case. The measured anisotropy values are presented in Fig. 5a and their evolution is compared with the stress ratio. A good agreement can be found between both parameters, i.e. as the axial strain increases, both stress ratio and anisotropy values increase and, subsequently, for the last two stages of loading both are seen to decrease. The same trend can also be observed for the evolution of the number of vectors presented in Fig. 5b. These observations suggest that the (local) strain hardening can be captured by the increase in the active contact regions and their clustering along the major principal stress; and further, the (local) subtle reduction of stress ratio within the plateau is accompanied by the decrease in these micro scale quantities. This finding highlights the relevance of the active contacts to link the macro response to the microscale phenomena.

Formation of stress chains

For the case of spherical particles in contact, the initial contact area is invariably a point, and this may explain the fact that the debate around whether to use force or stress to identify the load bearing grains has not received much attention previously. For real sand grains, however, the contact topologies arising from the irregular shaped grains, makes this investigation necessary. In this study, the grains forming the force chains were identified as being those transmitting a force value greater than three times the mean normal contact force, *i.e.*, 3×3.02N=9.06N. This selection resulted in the identification of approximately 200 grains belonging to the strong force network (6% of the total number of grains). The 200 grains with the highest internal stresses, using the von Mises criterion, were also filtered out (Fig. 6). The results revealed that only half (*i.e.* 47.8%) of grains were both in the force and in the stress networks. This mismatch between the grains carrying the highest forces and grains carrying the highest stresses suggests that the 'force chain' criterion may not be able to identify the more stressed grains. This observation is critical since grain breakage due to stress concentration may initiate outside the force chain and change the stability and self-organisation of the assembly.

CONCLUSIONS

The simulation of a sample with over 3,000 grains interacting in a finite-discrete element framework under triaxial compression is shown here to reproduce well the macroscopic response obtained from experiments. By assigning only elasticity to the individual grains, the non-linear plastic response of the specimen was reproduced based on grain deformation and granular reorganisation, according to frictional contact conditions based on experimental measurements only. Another innovative aspect of the modelling approach proposed here is the

representation of the numerical membrane using deformable thin-shell elements that enable a more realistic representation of the laboratory conditions.

The evolution of two microscale parameters, the active contact regions and the anisotropy of the distribution of the contact normal vectors are shown to capture well the macroscopic strain hardening and the stress ratio plateau of the material. It is also shown here that the grains experiencing the highest stresses are not necessarily part of the force chains network (i.e. those grains transmitting an above average force). The use of the 'stress chain' concept is discussed and proposed as a more suitable approach to consider grain breakage that may initiate outside the strong force network and compromise the stability of the assembly.

ACKNOWLEDGMENTS

The authors would like to acknowledge the provision of the Martian regolith-like sand associated to the National Science Foundation grant number ACI-1548562. Thanks also to City University of London for sponsoring the doctoral scholarship of the first author.

REFERENCES

Ahmad, S., Irons, B.M. & Zienkiewicz, O.C., (1970). Analysis of thick and thin shell structures by curved finite elements. International Journal for Numerical Methods in Engineering, 2(3), 419-451.

Andrade, J.E., Lim, K.W. Avila, C.F. & Vlahinić, I. (2012). Granular element method for computational particle mechanics. *Computer Methods in Applied Mechanics and Engineering*, 241, 262-274, ISSN 0045-7825.

Andò, E., Hall, S.A., Viggiani, G., Desrues, J. and Bésuelle, P., (2012). Grain-scale experimental investigation of localised deformation in sand: a discrete particle tracking approach. *Acta Geotechnica*, 7(1), pp.1-13.

Blumenfeld, R. & Ma J. (2017). Bending back stress chains and unique behaviour of granular matter in cylindrical geometries. *Granular Matter* **19**:29, DOI: 10.1007/s10035-017-0707-8

Binesh, S. M., Eslami-Feizabad, E., & Rahmani, R. (2018). Discrete Element Modeling of Drained Triaxial Test: Flexible and Rigid Lateral Boundaries. *International Journal of Civil Engineering*, 1-12.

Cavarretta, I., Coop, M. & O'Sullivan, C. (2010). The influence of particle characteristics on the behaviour of coarse grained soils. *Géotechnique* **60** (6): 413-423.

Cheung, G. & O'Sullivan, C. (2008). Effective simulation of flexible lateral boundaries in two and three-dimensional DEM simulations. *Particuology* **6**, No. 6, 483–500.

Cuccovillo, T. & Coop, M. R. (1999). On the mechanics of structured sands. *Géotechnique* 49, No. 6, 741–760, http://dx.doi.org/10.1680/geot.1999.49.6.741.

Cui, L., O'Sullivan, C. & O'Neill, S. (2007). An analysis of the triaxial apparatus using a mixed boundary three-dimensional discrete element model. *Géotechnique* **57**, No. 10, 831–844 [doi: 10.1680/geot.2007.57.10.831]

de Bono, J., McDowell, G. & Wanatowski, D. (2012). Discrete element modelling of a flexible membrane for triaxial testing of granular material at high pressures. *Géotechnique Letters* **2** (4):199–203.

Dassault Systèmes (2014). ABAQUS user's manual 2014 version 6.14. Providence, RI, USA: Dassault Systèmes.

Fonseca, J., O'Sullivan, C., Coop, M.R. & Lee, P.D. (2013). Quantifying the evolution of soil fabric during shearing using directional parameters. *Géotechnique* **63** (6): 487-499.

Fonseca, J., Nadimi, S., Reyes-Aldasoro, C.C, O'Sullivan, C. & Coop, M.R. (2016). Image-based investigation into the primary fabric of stress transmitting particles in sand, *Soils & Foundations* **56** (5): 818-834.

Gerritsen, M., Kreiss, G. & Blumenfeld, R. (2008). Stress chain solutions in two-dimensional isostatic granular systems: fabric-dependent paths, leakage, and branching. *Physical Review Letters* **101**, 098001.

Hall, S.A., Bornert, M., Desrues, J., Pannier, Y., Lenoir, N., Viggiani, G. and Bésuelle, P., 2010. Discrete and continuum analysis of localised deformation in sand using X-ray μCT and volumetric digital image correlation. *Géotechnique* **60** (5), pp.315-322.

Kawamoto, R., Andò, E., Viggiani, G., & Andrade, J. E. (2018). All you need is shape: Predicting shear banding in sand with LS-DEM. *Journal of the Mechanics and Physics of Solids*, 111, 375-392.

Krumbein, W. C., & Sloss, L. L. (1963). Stratigraphy and sedimentation, W.H. Freeman and Company, San Francisco.

Kuwano, R. & Jardine, R. J. (2002). On the applicability of cross-anisotropic elasticity to granular materials at very small strains. *Géotechnique* 52(10), 727–749, http://dx.doi.org/10.1680/ geot.2002.52.10.727.

Kong, D. & Fonseca, J. (2017). Quantification of the morphology of shelly carbonate sands using 3D images. *Géotechnique*, 68(3), 249-261 https://doi.org/10.1680/jgeot.16.P.278

Lu, Y., Li, X., & Wang, Y. (2018). Application of a flexible membrane to DEM modelling of axisymmetric triaxial compression tests on sands. *European Journal of Environmental and Civil Engineering*, 1-18.

Maeda, K., Sakai, H., Kondo, A., Yamaguchi, T., Fukuma, M. & Nukudani, E. (2010). Stress-chain based micromechanics of sand with grain shape effect. *Granular Matter* **12**:499–505. DOI: 10.1007/s10035-010-0208-5

Majmudar, T.S. & Behringer, R.P. (2005). Contact force measurements and stress-induced anisotropy in granular materials. *Nature* **435**, 1079-1082. DOI:10.1038/nature03805

Matsushima, T., & Chang, C. S. (2011). Quantitative evaluation of the effect of irregularly shaped particles in sheared granular assemblies. Granular matter, 13(3), 269-276.

Michalowski, R.L., Wang, Z. & Nadukuru, S.S. (2017). Maturing of contacts and ageing of silica sand. *Géotechnique*, http://dx.doi.org/10.1680/jgeot.16.P.321

Munjiza, A. (2004). *The combined finite-discrete element method*. West Sussex, England: John Wiley & Sons.

Nadimi, S. & Fonseca, J. (2017). Single grain virtualisation for contact behaviour analysis on sand. *Journal of Geotechnical and Geoenvironmental Engineering*, **143** (9), 06017010.

Nadimi, S. & Fonseca, J. (2018a). A micro finite element model for soil behaviour. *Géotechnique*, 68(4), 290-302 https://doi.org/10.1680/jgeot.16.P.147

Nadimi, S. & Fonseca, J. (2018b). A micro finite element model for soil behaviour: numerical validation. *Géotechnique*, 68(4), 364-369 http://doi.org/10.1680/jgeot.16.P.163

Nardelli, V., Coop, M. R., Andrade, J. E., & Paccagnella, F. (2017). An experimental investigation of the micromechanics of Eglin sand. Powder Technology, 312, 166-174

Ng, T.-T. (2004). Macro- and micro-behaviors of granular materials under different sample preparation methods and stress paths. Int. J. Solids Struct. 41, No. 21, 5871–5884.

Oda, M. & Iwashita, K. (1999). *Mechanics of granular materials, an introduction*. Rotterdam, the Netherlands CRC Press.

O'Sullivan, C. (2011). *Particulate Discrete Element Modelling: A Geomechanics Perspective*. Spon Press.

Radjai, F., Roux, J.N. & Daouadji, A. (2017). Modeling granular materials: century-long research across scales. *Journal of Engineering Mechanics* **143** (4), https://doi.org/10.1061/(ASCE)EM.1943-7889.0001196

Reese, S., Raible, T. & Wriggers, P., (2001). Finite element modelling of orthotropic material behaviour in pneumatic membranes. International journal of solids and structures, 38(52), 9525-9544.

Satake, M. (1982). Fabric tensor in granular materials. In IUTAM Conference on Deformation and Flow of Granular Materials, 1982 (pp. 63-68). AA Balkema.

Shewchuk, J. R. (2014). Reprint of: Delaunay refinement algorithms for triangular mesh generation. *Computational Geometry: Theory and Applications* **47** (7): 741-778.

Sze, K.Y., (2002). Three-dimensional continuum finite element models for plate/shell analysis. *Progress in Structural Engineering and Materials*, 4(4),400-407.

Vlahinić, I., Andò, E., Viggiani, G., Andrade, J.E. (2013). Towards a more accurate characterization of granular media: extracting quantitative descriptors from tomographic images. *Granular Matter* **16** (1), 9-21.

Wang, L. B., Frost, J. D., & Lai, J. S. (2004). Three-dimensional digital representation of granular material microstructure from X-ray tomography imaging. *Journal of Computing in Civil Engineering*, 18(1), 28-35.

Wiebicke, M., Andò, E., Herle, I., & Viggiani, G. (2017). On the metrology of interparticle contacts in sand from x-ray tomography images. *Measurement Science and Technology*, 28(12), 124007.

Yang, Z. X., & Wu, Y. (2016). Critical state for anisotropic granular materials: a discrete element perspective. *International Journal of Geomechanics*, 17(2), 04016054

Zhang, Y., Shao, J., Liu, Z., Shi, C., & De Saxcé, G. (2018). Effects of confining pressure and loading path on deformation and strength of cohesive granular materials: a three-dimensional DEM analysis. *Acta Geotechnica*, 1-18.

FIGURES

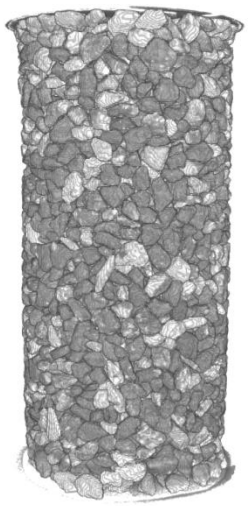

(a)

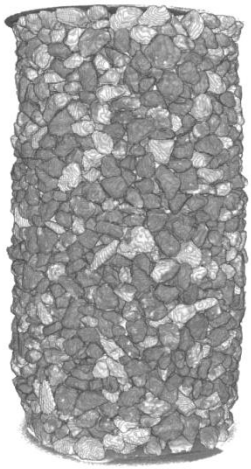

(b)

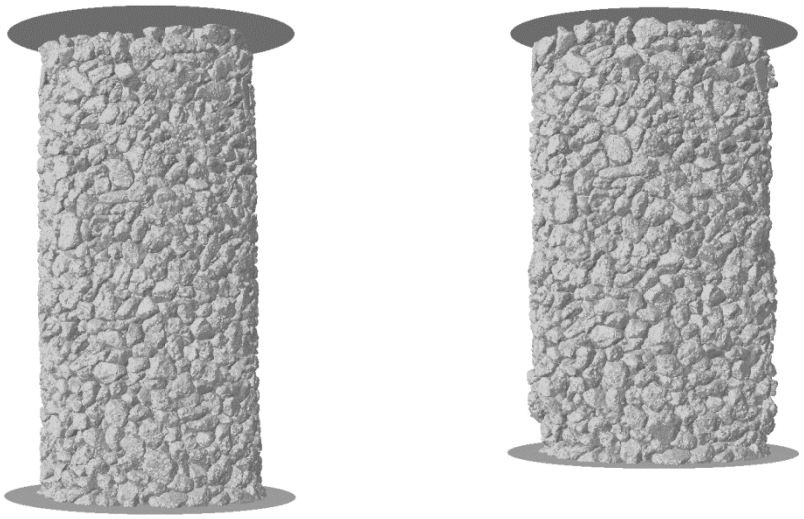

(c) (d)

Fig. 1. Views of the full experimental specimen at: (a) 0% axial strain and (b) 10% axial strain and of the numerical specimen at: (c) 0% axial strain and (d) 10% axial strain

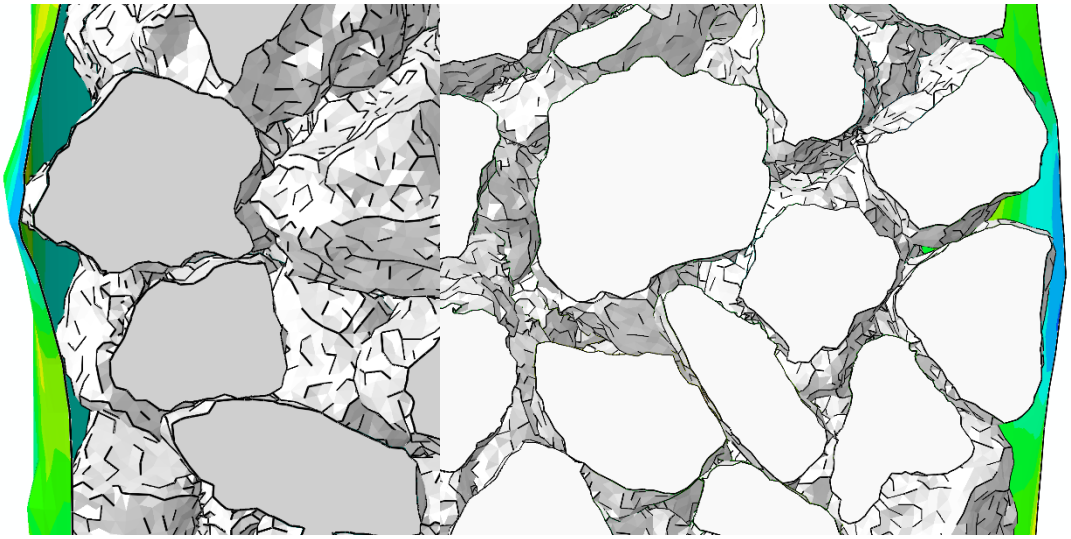

(a) (b)

Fig. 2. Detailed views showing the deformation in the membrane and the strain concentration, represented here by darker shades in the membrane, (a) left side of the cross- section, and (b) right side of the cross-section

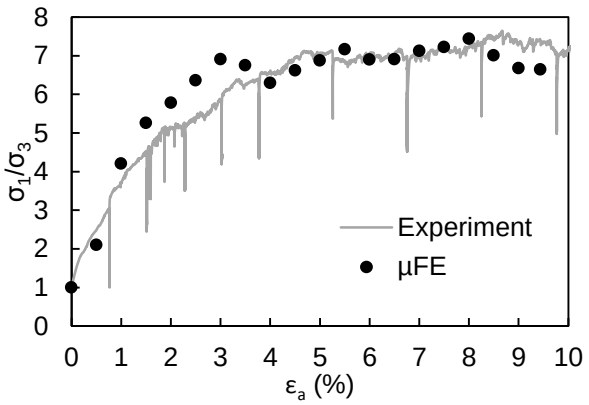

(a)

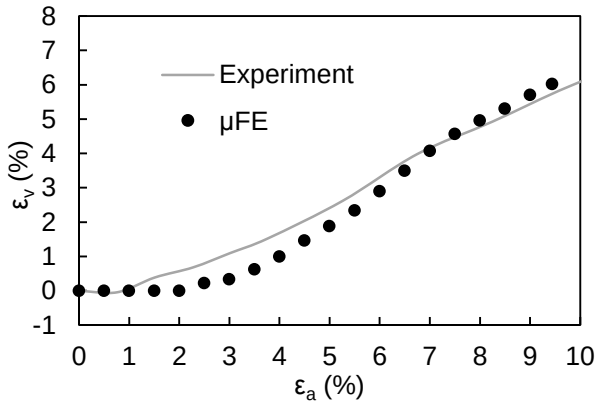

(b)

Fig. 3. Comparison between the macroscopic results from the μFE model and the experiments: (a) Stress-strain response and (b) Volumetric response

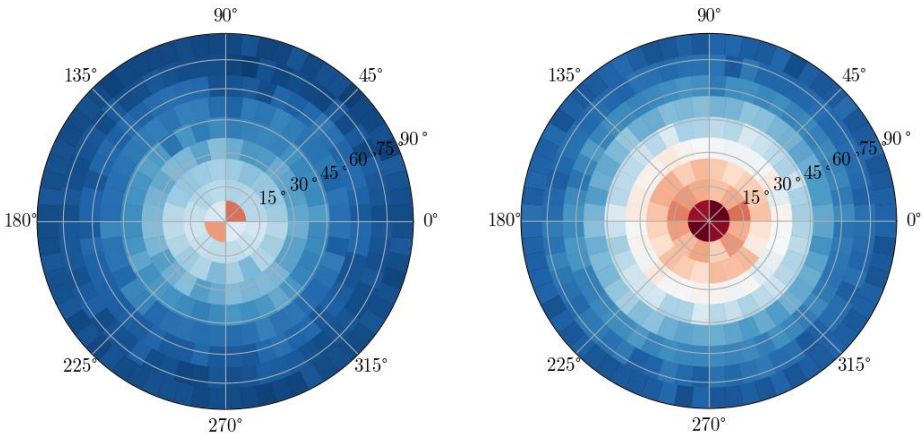

(a) (b)

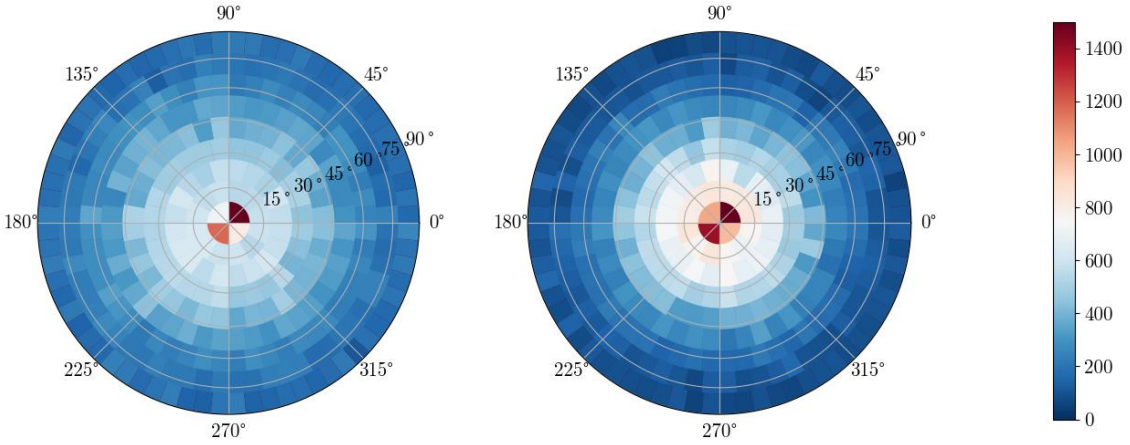

(c) (d)

Fig. 4. Polar plots showing the evolution of contact normal vectors for: (a) axial strain level of 2.5% number of vectors of 105744, (b) strain 5.5% no. vectors 129431, (c) strain 7.5% no. vectors 93160, (d) strain 9.5% no. vectors 69078

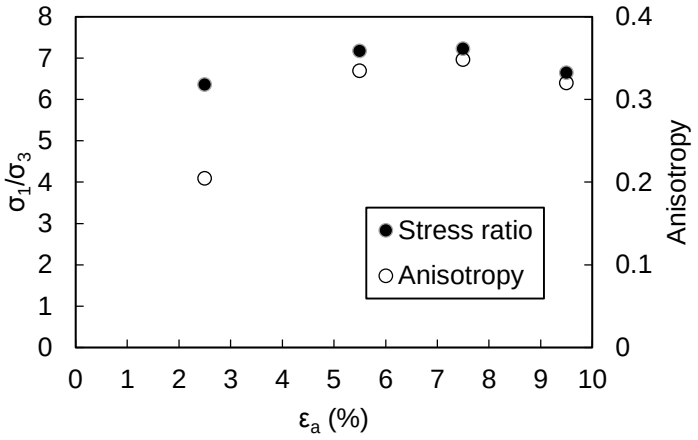

(a)

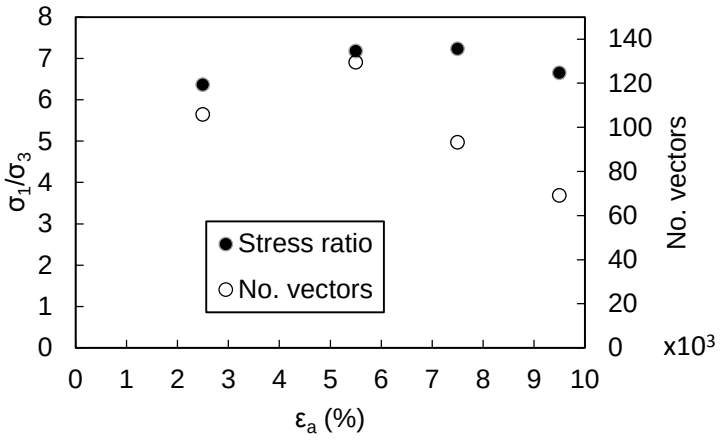

(b)

Fig. 5. Comparison of the evolution of the stress ratio with two micro scale parameters: (a) anisotropy of the distribution of the contact normal vectors, (b) number of contact normal vectors

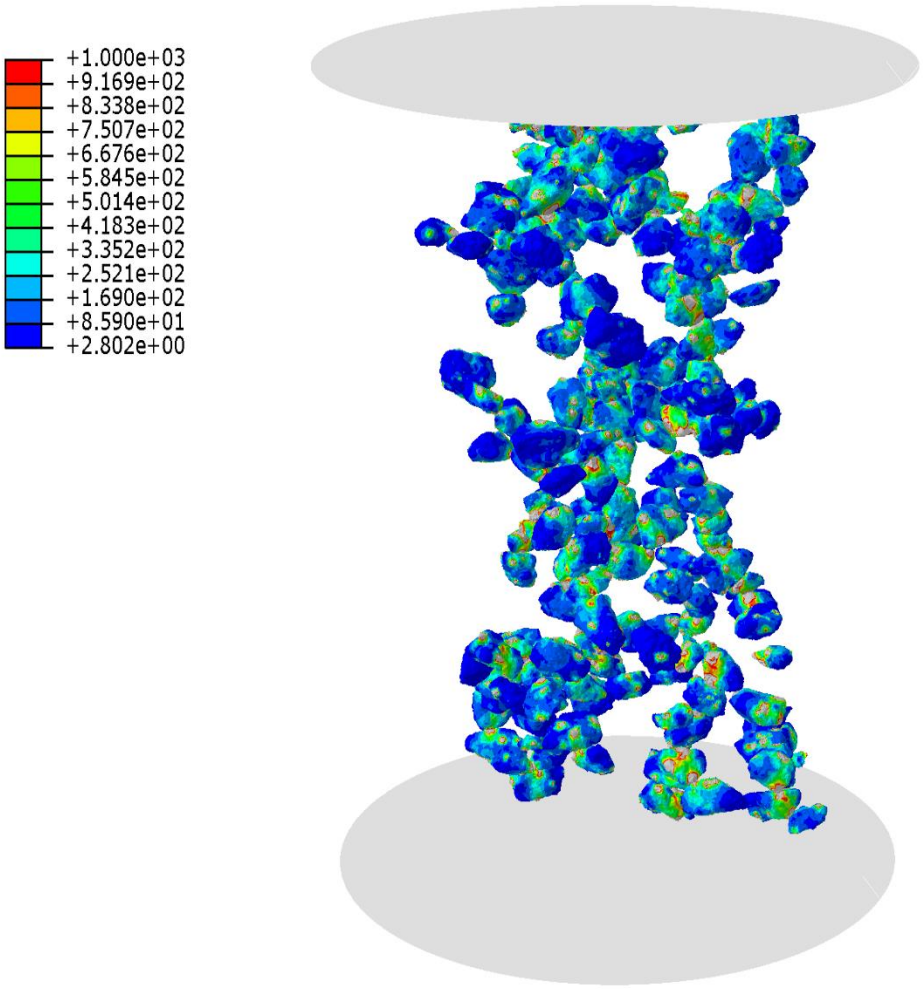

Fig. 6. Display of the stress chains at 9.5% strain for the 200 most stressed grains in the numerical sample. The stress distribution was calculated using the von Mises criterion, units are in MPa.